Three-Dimensional Activity Volcano Plot under an External Electric Field

Changming Ke, Zijing Lin, and Shi Liu*

Read Online

ACCESS | Metrics & More | Article Recommendations | Supporting Information

ABSTRACT: An external electric field (EEF) can impact a broad range of catalytic processes beyond redox systems. Computational design of catalysts under EEFs targeting specific operation conditions essentially requires accurate predictions of the response of a complex physicochemical system to collective parameters such as EEF strength/direction and temperature. Here, we develop a multiscale approach that progressively bridges finite-field density functional theory, chemical reaction network theory, microkinetic modeling, and machine learning-assisted high-throughput computations, which leads to the construction of a three-dimensional activity volcano plot under EEFs for thousands of metallic alloys. Taking steam reforming of methanol as an example, we discover a nontrivial collective effect of EEF and temperature on the conversion of methanol: a positive EEF can increase the conversion at high temperatures but strongly suppress the conversion at low temperatures, highlighting the necessity of multiscale modeling for catalyst design under EEFs.

KEYWORDS: *electrostatic catalysis, 3D activity volcano plot, catalysis design, deep learning, steam reforming of methanol, microkinetics*
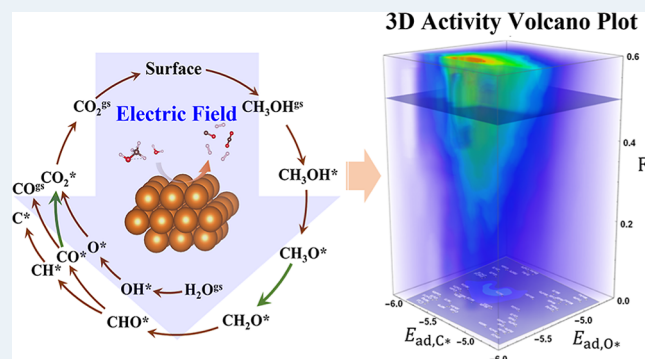
■ INTRODUCTION

Much like Earth's climate and spin glass, heterogeneous catalysis is an archetypal complex system and plays a pivotal role in our society. Electric field (EF) can manipulate the chemical reactivity and selectivity by tuning the relative stability of polar or ionic reactants and/or transition states in chemical reactions beyond redox systems,[1−6] opening up exciting opportunities to control catalytic reactions in an on-demand manner using EFs, hereinafter referred to as electrostatic catalysis. Achieving predictability of complex dynamical systems is one of the most challenging problems in physics. Similarly, to take full advantage of electrostatic catalysis, a fundamental challenge is to predict the response of heterogeneous catalysis, a complex physicochemical system involving a network of chemical reactions and physical processes, to collective reaction parameters, specifically field strength and temperature.

The presence of an EF under realistic reaction conditions can have both intrinsic and extrinsic origins.[2,4,6,7] It is more convenient in practice to directly apply an external EF (EEF) to a reactor as the strength and direction of the field is readily tunable. To apply EEFs in large-scale reactions, several reactor systems have been developed.[8−10] For example, probe−bed−probe reactors have a conductive catalyst bed placed in the gap between two external probes. The only additional energetic cost of electrostatic catalysis is for one-time charging a capacitor that maintains the high voltage across the probes.[3]

The catalyst bed often consists of catalytically active metal nanoparticles that can generate very high surface EFs in the presence of EEFs by virtue of the curvature-induced field enhancement effect.[11] For example, an EF of 0.1 V/Å can be generated by a 1 V voltage near the surface of a 1 nm nanoparticle.[3] Additionally, surface EFs are always perpendicular to the metal surface, potentially allowing for a fine control of the relative orientation between the EEF and adsorbed molecules. Therefore, understanding the effects of EEFs on heterogeneous catalysis by metals is a major focus of electrostatic catalysis.[11−13]

Methanol, as an important hydrogen-storage liquid fuel,[14] can be used for hydrogen production through steam reforming of methanol (SRM),[15] in which methanol reacts with steam and produces hydrogen, CO, and CO$_2$ at about 300 °C. It is expected that a cost-effective SRM process will be crucial for a hydrogen-based renewable energy future. However, the extensively used catalysts in industries such as Cu often suffer from catalyst deactivation due to coke deposition and sintering.[16] Moreover, to integrate the SRM process with
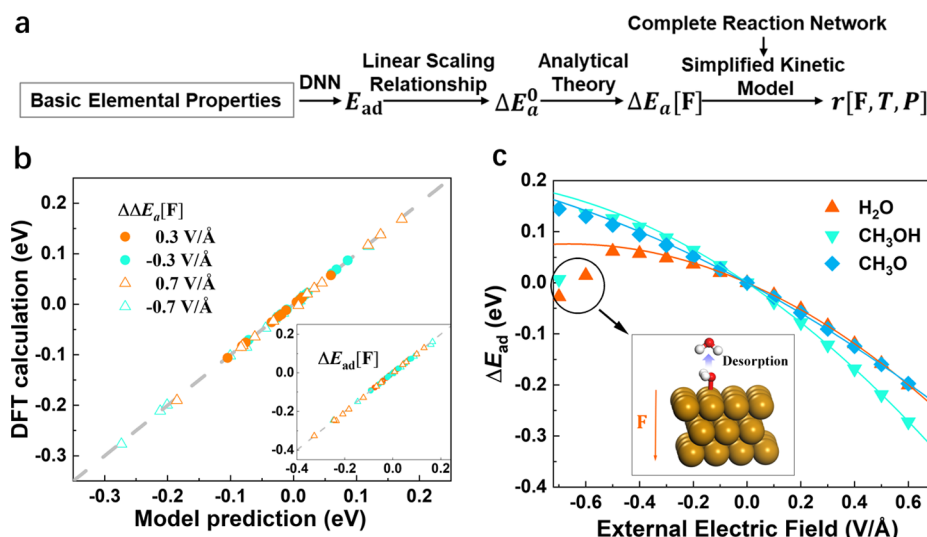
Figure 1. (a) Workflow of a multiscale approach that predicts the reaction rate (r) under realistic conditions specified by temperature (T), partial pressures of reactants (P), and an external electric field ($\mathbf{F}$). The analytical theory derived within the harmonic approximation enables rapid and accurate predictions of finite-field activation energy ($\Delta E_a[\mathbf{F}]$) using only zero-field activation energy (ΔE_a^0). (b) Comparison of EEF-induced activation energy change ($\Delta\Delta E_a[\mathbf{F}]$) and adsorption energy change ($\Delta E_{ad}[\mathbf{F}]$) estimated with the analytical relationships and direct DFT calculations for tightly bonded adsorbates and transition states. (c) Comparison of analytical (solid lines) and DFT (scattered dots) values of $\Delta E_{ad}[\mathbf{F}]$ for three representative species. The inset shows H_2O will desorb from the surface due to a strong negative field.

proton-exchange membrane fuel cells for vehicle propulsion and power generation, it is desirable to have SRM operating at low temperatures (<200 °C) for improved safety and energy efficiency.[17] Another benefit of low-temperature SRM is the suppression of CO production to avoid CO poisoning of catalysts in fuel cells; CO molecules adsorbed on the surface of a catalyst will be oxidized to CO_2 due to the low desorption rate.[18,19] Unfortunately, most catalysts for high-temperature SRM have poor reactivities below 200 °C.[16] Because the elementary reactions of SRM involve adsorbates possessing large electric dipole moments, we expect that an EEF will bring appreciable impacts on the kinetics and thermodynamics of the SRM process as the energetics of molecules of large electric dipole moments are susceptible to EEFs.[5,20] In view of the critical role of SRM played in the green methanol economy,[14,21] it is imperative to design next-generation catalysts superior to the current ones, particularly for low-temperature SRM. In this work, we propose to use EEF as a "smart agent" to improve the catalytic activity and coke resistance.

First-principles-based computational catalyst design is emerging as a promising approach to obtain high-quality catalysts.[22−24] Pertinent to electrostatic catalysis, finite-field density functional theory (DFT) calculations have been used to quantify the activation energies (ΔE_a) of elementary reactions on metal surfaces in the presence of EEFs of varying magnitudes, revealing important atomistic insights that helped the understanding of EEF effects.[3,13,25] However, most previous studies only focused on a few representative electric fields (e.g., negative vs positive) and their impact on the catalytic activity of a specific metal (e.g., Ni, Ag),[13,25] partly due to the expensive computational cost of finite-field DFT calculations. For a complex process, like SRM comprising a network of elementary reactions, the EEF dependence of the overall catalytic performance is likely nonlinear such that the search of an optimal EEF should be performed in order to maximize the efficiency but has never been done. Moreover,

the design of high-quality electrostatic catalysts targeting specific operation conditions requires detailed understandings of the collective effects of EEFs and various reaction parameters, such as temperature, gas composition, and partial pressure. All these difficulties essentially forbid a DFT-based high-throughput computational catalyst screening in the presence of EEFs.

Here, using SRM as an example, we develop a deep-learning-assisted first-principles-based multiscale method that leads to a three-dimensional (3D) activity volcano plot under EEFs, quantifying the field-dependent SRM activity for thousands of metallic alloys. The multiscale approach is illustrated in Figure 1a. A DFT-based deep neural network (DNN) is employed to rapidly predict C* and O* adsorption energies (E_{ad}) using basic elemental properties,[22] which are then used to compute the activation energies (ΔE_a^0) of key elementary reactions at the zero field based on the linear scaling relationship.[26,27] Importantly, we derive an analytical theory that relates the finite-field activation energies ($\Delta E_a[\mathbf{F}]$) to field strength ($\mathbf{F}$) and ΔE_a^0 within the harmonic approximation. The predicted finite-field energetics and reaction parameters, such as temperatures and partial pressures of reactants, are inputs of a simplified kinetic model that captures the essence of the complete reaction network. Finally, guided by a 3D activity volcano plot obtained from the multiscale modeling, we identify high-quality catalysts for low-temperature SRM under EEFs. Moreover, we discover a highly nonlinear temperature-dependent EEF effect: a positive EEF can increase the conversion of CH_3OH at high temperatures (>350 °C) but suppress the conversion at low temperatures (<250 °C), highlighting the necessity of multiscale modeling for catalyst design under EEFs.

■ METHODS

DFT calculations are performed using Vienna ab initio Simulation Package (VASP).[28,29] The interaction between the core ion and electrons is described by the projector
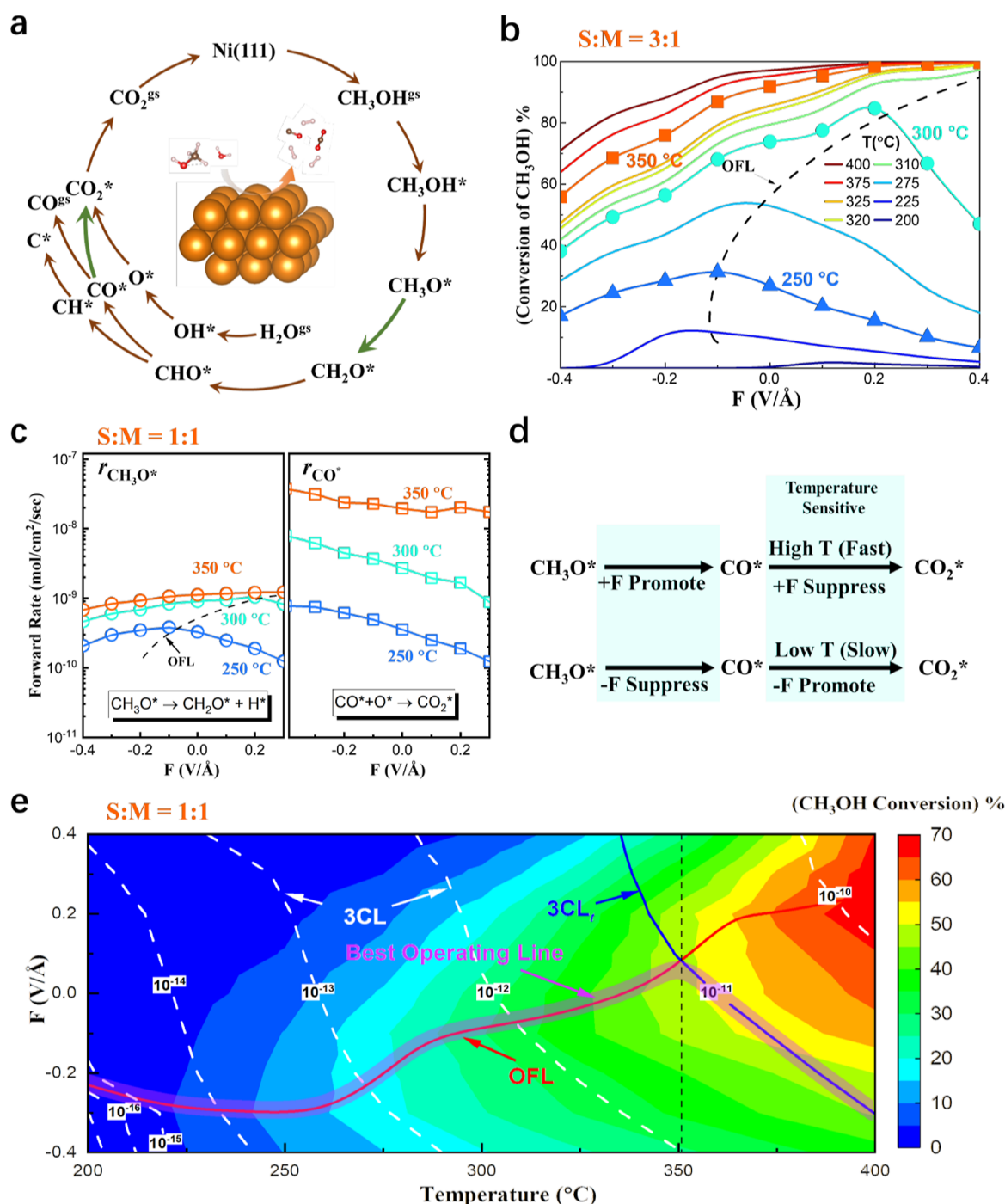
Figure 2. Nonlinear temperature-dependent EEF effect in SRM. (a) Reaction network of SRM considered in this work. The green arrows highlight two RDSs. (b) Methanol conversion as a function of electric field strength at different temperatures for a 3:1 steam to methanol ratio (S/M = 3:1). (c) Field and temperature dependence of $r_{CH_3O^*}$ and r_{CO^*}. (d) Mechanisms responsible for the nonlinear temperature-dependent EEF effect. (e) Contour plot of methanol conversion as a function of temperature and field strength for S/M = 1:1, showing OFL (red line) and constant carbon concentration lines (3CLs, white dashed lines). For a target level of coke resistance denoted as $3CL_t$, the lower part of the merged OFL and $3CL_t$ (shaded pink line) gives the best operating line for a wide range of temperatures.

augmented wave method.[30] The Perdew-Wang-91 (PW91) functional is chosen as the exchange−correlation functional.[31] The plane-wave kinetic energy cutoff is 400 eV and a 5 × 5 × 1 Monkhorst−Pack grid is used to sample the Brillouin zone. A three-layer 3 × 3 Ni slab with a vacuum region of more than 10 Å thick is constructed to simulate the Ni(111) surface. The method proposed by Neugebauer and Scheffler[32] is employed to apply an EEF normal to the metal surface. Climbing image-

nudged elastic band method[33] and dimer method[34] are used to identify transition states of surface reactions, and the electronic energy and atomic force are converged, respectively, to 10^{-7} eV and 0.01 eV/Å. More computational details can be found in the Supporting Information. All codes and data can be downloaded from a public repository.[35]

■ RESULTS AND DISCUSSION

Finite-Field Energetics within the Harmonic Approximation. One main hurdle for high-throughput computational screening of EEF-assisted catalysts is due to the expensive computational cost of finite-field DFT calculations. For an elementary surface reaction step, the EEF-induced changes in adsorption and activation energy have been attributed to various factors such as modified charge transfer between adsorbates and metal surfaces,[36] bond elongation/contraction of adsorbates, as well as the shift of metal work function.[37] These important yet intimately coupled atomistic mechanisms seem to suggest a quantitative determination of the EEF-induced energy change can only be achieved via genuine ab initio modeling that captures all the mentioned factors. We now show that $\Delta E_a[\mathbf{F}]$ at a given field ($\mathbf{F}$) can be readily obtained using only zero-field parameters within the harmonic approximation.

Without loss of generality, a simple elementary reaction, R* → TS* → P* is considered, where R*, TS*, and P* are the reactant, transition state, and product adsorbed on the metal surface, respectively, and the EEF is applied along the surface normal. For an isolated species i under an EEF, its free energy in the form of Taylor series up to the second order is

$$E_i[\mathbf{F}] = E^0 - \mathbf{d}_i \cdot \mathbf{F} - \frac{1}{2}\alpha_i \mathbf{F}^2 \tag{1}$$

where E^0 is the zero-field energy, $\mathbf{d}$ is the dipole moment, and α is the polarizability. Equation 1 applies to both isolated molecules as well as the slab model with adsorbates (denoted as $s + i$). It is straightforward to derive

$$\Delta E_a[\mathbf{F}] = \Delta E_a^0 - (\mathbf{d}_{s+\text{TS}*} - \mathbf{d}_{s+\text{R}*}) \cdot \mathbf{F}$$
$$- \frac{1}{2}(\alpha_{s+\text{TS}*} - \alpha_{s+\text{R}*})\mathbf{F}^2 \tag{2}$$

where $\Delta E_a^0 = E_{s+\text{TS}*}^0 - E_{s+\text{R}*}^0$ is the zero-field activation energy. We note that $\mathbf{d}_{s+\text{TS}*}$ and $\alpha_{s+\text{TS}*}$ ($\mathbf{d}_{s+\text{R}*}$ and $\alpha_{s+\text{R}*}$) are the electric dipole moment and polarizability, respectively, of the whole bounded system composed of the adsorbed TS* (R*) and the slab used to model the surface. It is evident that all reaction-specific parameters (ΔE_a^0, $\mathbf{d}$, α) in eq 2 can be computed from DFT and perturbation theory at the zero field. A generalization of eq 2 gives the adsorption energy under EEFs

$$E_{\text{ad}}[\mathbf{F}] = E_{\text{ad}}^0 - (\mathbf{d}_{s+i} - \mathbf{d}_s) \cdot \mathbf{F} - \frac{1}{2}(\alpha_{s+i} - \alpha_s)\mathbf{F}^2 \tag{3}$$

where $E_{\text{ad}}^0 = E_{s+i}^0 - E_s^0 - E_i^0$ is the zero-field adsorption energy. We note that our definition of adsorption energy captures the effect of EEF-driven gas diffusion and is subtlety different from the conventional definition (see details in Supporting Information, Sect. II).

Expressions similar to eqs 2 and 3 have been derived previously[3,25] but, surprisingly, have never been used to calculate $\Delta E_a[\mathbf{F}]$ or $E_{\text{ad}}[\mathbf{F}]$, likely because of the general assumption that EEF-induced structural and electronic changes of metal surface−adsorbate complex would be highly anharmonic. We compare the EEF-induced energy change, $\Delta\Delta E_a[\mathbf{F}] = \Delta E_a[\mathbf{F}] - \Delta E_a^0$ and $\Delta E_{\text{ad}}[\mathbf{F}] = E_{\text{ad}}[\mathbf{F}] - E_{\text{ad}}^0$, obtained with eqs 2 and 3 using only zero-field parameters and those from direct DFT calculations in Figure 1b. With mean absolute errors of only 1 meV and 2 meV for $\Delta\Delta E_a[\mathbf{F}]$ and $\Delta E_{\text{ad}}[\mathbf{F}]$, respectively, the simple analytical relationships

described by eqs 2 and 3 have remarkable accuracy over a wide range of field strengths. We further compare the analytical and DFT values of $\Delta E_{\text{ad}}[\mathbf{F}]$ for three representative molecules, H_2O, CH_3OH, and CH_3O in Figure 1c and find a satisfying agreement for $-0.4 < \mathbf{F} < 0.7$ eV/Å. Consistent with previous DFT investigations,[3,38] a negative field may induce desorption ($\Delta E_{\text{ad}}[\mathbf{F}] > 0$), while a positive field facilitates the adsorption ($\Delta E_{\text{ad}}[\mathbf{F}] < 0$) for a molecule with a negative electric dipole moment on a metal surface. It is only when the molecules become desorbed due to a strong negative field (e.g., -0.5 V/Å for H_2O) that the analytical value of $\Delta E_{\text{ad}}[\mathbf{F}]$ starts deviating from the DFT result. We note that an EEF in principle could affect the polarizability α_i, but this higher order term does not contribute substantially to the change in energy at relatively low electric fields.

The demonstrated quantitative nature of a rather simple analytical theory linking the field strength to the EEF-induced energy change seems counterintuitive. From eqs 2 and 3, it is clear that only the whole bounded system (the slab with an adsorbed molecule) is relevant to EEF-dependent terms. We argue that for the whole bounded system, the impact of an EEF on the total energy is a small perturbation that could be well described within the harmonic approximation, despite highly anharmonic local changes between the adsorbate and the metal surface (see additional discussions in Supporting Information, Sect. III).

Microkinetics of SRM under EEFs. The reaction network of SRM, as illustrated in Figure 2a, includes CH_3OH and H_2O dehydrogenation and CO* oxidation, and the products include H_2, CO, and CO_2. Based on eqs 2 and 3, we construct a microkinetic model (see details in Supporting Information, Sect. V) that simulates the Ni-catalyzed SRM process in the presence of EEFs under realistic conditions that take into account the impacts of gas composition, temperature, and inlet velocity. For a 3:1 steam to methanol ratio (S/M = 3:1), the temperature- and field-dependence of the conversion of CH_3OH is presented in Figure 2b, where we define an "optimal field line" (OFL) that tracks the electric field resulting in the highest conversion ($\mathbf{F}_{\text{OF}}$). The OFL reveals several interesting characteristics of SRM under EEFs. At high temperatures ≥310 °C, a positive field can promote the conversion compared to the zero-field case, and the degree of enhancement scales with the field strength. Interestingly, at an intermediate temperature, such as 300 °C, a large positive field that is to the right of the OFL will suppress the conversion. When the OFL crosses the zero field and enters into the negative field region, it means a negative field now can facilitate the conversion; this happens at ≈ 250 °C, but a too strong negative field also becomes unfavorable.

We perform sensitivity analysis by computing the partial derivatives of methanol conversion rate with respect to the rate constant of individual elementary reaction.[39] Two rate-determining steps (RDSs) are found in SRM, the dehydrogenation of CH_3O*, $CH_3O* + * \rightarrow CH_2O*+H*$ and the consumption of CO*, $CO* + O* \rightarrow CO_2*$. The nontrivial evolution of OFL is due to a delicate balance between the two RDSs with the consumption rate of CO* ($r_{\text{CO}*}$) being more temperature sensitive than the dehydrogenation rate of CH_3O* ($r_{\text{CH}_3\text{O}*}$). As shown in Figure 2c, a positive EEF always suppresses $r_{\text{CO}*}$, whereas it mostly promotes $r_{\text{CH}_3\text{O}*}$. At a high temperature of 350 °C, the overall rate of SRM is dictated by $r_{\text{CH}_3\text{O}*}$ ($\approx 10^{-9}$ mol/cm²/s) as $r_{\text{CO}*}$ is fast enough ($>10^{-8}$
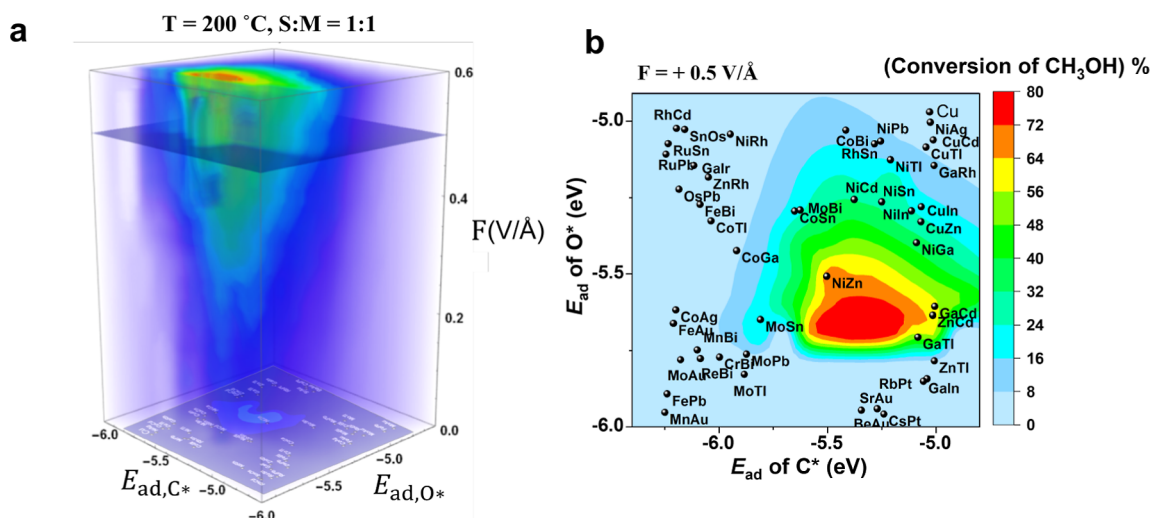
Figure 3. (a) 3D activity volcano plot for SRM at 200 °C and S/M = 1:1 under EEFs with a slice of **F** = 0.5 V/Å shown in (b). The flow rate is 10 mL/min and the activation surface of the catalyst is 0.14 m², same as the experimental setup in ref 42. The high feed rate will cause CO poisoning for most known SRM catalysts such as Cu. Results for a low ratio of the flow rate to the activation surface are plotted in Figure S11 where Cu-based catalysts are active.

mol/cm²/s) for |**F**| < 0.4 V/Å. Therefore, the methanol conversion simply scales with the strength of the positive EEF (Figure 2b). When the temperature is lowered to 300 °C, r_{CO*} remains fast ($r_{CH_3O*} < r_{CO*}$) such that applying a positive EEF below the optimal field $\mathbf{F}_{OF}$ can still facilitate the conversion by increasing r_{CH_3O*}. However, after exceeding $\mathbf{F}_{OF}$, the speed of CO* generation from CH₃O* dehydrogenation will become comparable with the speed of CO* consumption, and CO poisoning of Ni starts hindering the SRM process. This explains the concave downward feature of the field dependence of the methanol conversion at 300 °C (Figure 2b). At a low temperature of 250 °C, the zero-field CO* consumption rate becomes rather slow thus requiring a negative field to promote r_{CO*}; a too strong negative field that severely reduces r_{CH_3O*} will unsurprisingly cause a low methanol conversion. Simply put, the OFL essentially marks the boundary between the CH₃O*-dehydrogenation-controlled region and CO-poisoning-controlled region, with the mechanisms depicted in Figure 2d. Similar concave downward features of the field dependence of the reaction rate have been observed experimentally in Pt-catalyzed steam reforming of methane,[8] hinting at a common feature for EFF-assisted catalysis.

It is well known that coking (the formation of carbon that covers active sites) is the most common deactivation mechanism of industrial SRM catalysts,[40,41] and increasing the steam pressure is the general approach to suppress coking. Though a high S/M ratio (e.g., 3:1) is beneficial for enhancing coke resistance, it will raise energy consumption for steam heating, reduce the methanol conversion, and decrease the H₂ content of the final products. It would be helpful to have an efficient tool to identify the optimal conditions for the balanced SRM rate and coke resistance. For S/M = 1:1, we construct a contour plot of methanol conversion as a function of the temperature and EEF strength (Figure 2e), showing both OFL and constant carbon concentration lines (3CLs). Because the C* generation by the dehydrogenation of CH* is considered in our model (Figure 2a), we can readily obtain the C* concentration at a reaction condition specified by T and **F**. A 3CL traces the reaction conditions that yield the same C*

concentration. For a target level of coke resistance (a selected 3CL, denoted as 3CL$_t$), the lower part of the merged OFL and 3CL$_t$ gives the best operating EEF for a wide range of temperatures.

3D Activity Volcano Plot under EEFs. It is impractical to perform microkinetic modeling based on the complete reaction network during a high-throughput screening. We find that the microkinetic model of SRM in the presence of EEFs can be simplified as

$$CH_3OH \leftrightarrows CH_3OH^* \leftrightarrows CH_3O^* \xrightarrow{k^{RDS1}} CH_2O^* \leftrightarrows CHO^*$$

$$\leftrightarrows CO^* + O^* \xrightarrow{k^{RDS2}} CO_2^*$$
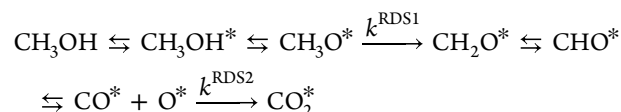
in which CH₃O* + * → CH₂O* + H* and CO* + O* → CO₂* are the RDSs, and ⇌ denotes equilibrium. The simplified kinetic model, taking the activation energies of those two RDSs at **F** as the only required inputs, is capable of rapidly predicting methanol conversion under a given reaction condition specified by the temperature and partial pressures of reactants (P_{CH_3OH} and P_{H_2O}). Detailed derivations to the simplified kinetic model can be found in Supporting Information, Sect. VIII.

Another challenge for constructing the activity volcano plot under EEFs for a large number of metallic catalysts is the prerequisite to predict $E_{ad}[\mathbf{F}]$ and $\Delta E_a[\mathbf{F}]$ on various metal surfaces accurately and rapidly. We find that the EEF-induced energy change turns out to be rather insensitive to the metal type (see more discussions regarding this seemingly counter-intuitive feature in Supporting Information, Sect. IX), which greatly simplifies the problem. That is, for an adsorbate i on a given metal surface (m), the field-dependent adsorption energy is reduced to $E_{ad}[\mathbf{F}, m] = E_{ad}^0[m] - (\mathbf{d}_{s_0+i} - \mathbf{d}_{s_0}) \cdot \mathbf{F} - \frac{1}{2}(\alpha_{s_0+i} - \alpha_{s_0})\mathbf{F}^2$, where $E_{ad}^0[m]$ is the zero-field adsorption energy on metal m that can be estimated using C* and O* adsorption energies on metal m with the well-known linear scaling relationship[22] while the last two terms only depend on **F** and are computed using a reference metal surface s_0. Equipped with a DNN that can quickly predict the zero-field adsorption energies of C* and

O* for various metallic alloys (see details in Supporting Information, Sect. X) and the simplified kinetic model, we finally construct a 3D activity volcano plot that quantitatively predicts the menthol conversion in the presence of EEFs for 1711 metallic alloys (Figure 3) at a low temperature of 200 °C, S/M = 1:1, flow rate of 10 mL/min, and an activation surface area of 0.14 m^2 (reaction conditions take from ref 42). This 3D volcano plot contains rich information and is worthy of detailed investigations. Here, we only highlight the catalytic performance of NiZn. Despite having a low SRM activity (<5%) at the zero field, NiZn can promote the methanol conversion (>60%) in the presence of an EEF of 0.5 V/Å at 200 °C. Combined with its proved coke resistance,[22] EEF-assisted NiZn is recommended as an efficient and environmentally friendly catalyst for SRM at 200 °C and S/M = 1:1.

We now make a few general comments regarding the limitations of the multiscale approach and propose strategies for further improvement. First, the possible surface reconstruction of metals and alloys with or without EEF was not considered. Given that understanding the surface reconstruction and its impact on heterogeneous catalysis by itself is a challenging problem, we are not claiming that the multiscale approach developed here has already captured this important aspect, though it is possible to incorporate surface reconstruction into the multiscale approach by developing a more sophisticated DNN model. Second, we made a few approximations (i.e., harmonic approximation and two RDSs) at different levels in order to enable high-throughput multiscale simulations. Each approximation comes with uncertainty in simulation results, and their collective effects across the models/scales on the final prediction, at this point, is difficult to quantify. With that said, the reasonable experiment−theory agreement as demonstrated in Supporting Information, Figure S7, suggests that the error cancellation likely works in our favor. More efforts are needed to develop a reliable protocol to quantify the propagation of error in the multiscale approach. We believe our current multiscale approach has a sufficient accuracy for high-throughput materials pre-screening to facilitate the design of new catalysts.

CONCLUSIONS

In summary, we demonstrate that a simple analytical theory within the harmonic approximation can accurately predict finite-field energetics using only zero-field parameters, eliminating the needs of expensive finite-field DFT calculations for field-dependent microkinetic modeling. Focusing on an important process in the green methanol economy, steam reforming of methanol, we reveal nontrivial collective effects of EEF and temperature: a positive EEF enhances the methanol conversion at higher temperatures while suppressing the overall reaction at lower temperatures. The introduction of OFL and 3CL$_t$ that quantifies the coke formation in the temperature−EEF parameter space allows for facile determinations of the best operating EEFs for a wide range of temperatures. Finally, using a chemistry-based simplified kinetic model and a first-principles-based DNN, we construct a 3D activity volcano plot under EEFs for 1711 metallic alloys and identify EEF-assisted NiZn for low-temperature steam reforming of methanol. We expect the multiscale approach developed in this work can be readily applied to other heterogeneous catalysis by metals under EEFs.

ASSOCIATED CONTENT

ⓈI Supporting Information

The Supporting Information is available free of charge at https://pubs.acs.org/doi/10.1021/acscatal.2c04961.

Weak EEF dependence of frequency factor, definition of adsorption energy under an EEF, analytical model verification for a EEF-sensitive structure, dipole moment and polarizability of adsorbates and transition states in SRM, microkinetics of EEF-assisted SRM on Ni(111), EEF effect on selectivity of CO, reaction fluxes of water gas shift, simplified kinetic model, linear scaling relationship in SRM, DNN model parameters, and validation of predicted volcano plot (PDF)

AUTHOR INFORMATION

Corresponding Author

Shi Liu − *Key Laboratory for Quantum Materials of Zhejiang Province, Department of Physics, School of Science and Research Center for Industries of the Future, Westlake University, Hangzhou 310030 Zhejiang, China; Institute of Natural Sciences, Westlake Institute for Advanced Study, Hangzhou 310024 Zhejiang, China;* ⓞ orcid.org/0000-0002-8488-4848; Email: liushi@westlake.edu.cn

Authors

Changming Ke − *Key Laboratory for Quantum Materials of Zhejiang Province, Department of Physics, School of Science and Research Center for Industries of the Future, Westlake University, Hangzhou 310030 Zhejiang, China; Institute of Natural Sciences, Westlake Institute for Advanced Study, Hangzhou 310024 Zhejiang, China*

Zijing Lin − *Hefei National Laboratory for Physical Sciences at Microscales, CAS Key Laboratory of Strongly-Coupled Quantum Matter Physics, Department of Physics, University of Science and Technology of China, Hefei 230026, China;* ⓞ orcid.org/0000-0001-9270-1717

Complete contact information is available at:
https://pubs.acs.org/10.1021/acscatal.2c04961

Notes

The authors declare no competing financial interest.

ACKNOWLEDGMENTS

REFERENCES

(1) Shaik, S.; Mandal, D.; Ramanan, R. Oriented electric fields as future smart reagents in chemistry. *Nat. Chem.* **2016**, *8*, 1091−1098.

(2) Shaik, S.; Ramanan, R.; Danovich, D.; Mandal, D. Structure and reactivity/selectivity control by oriented-external electric fields. *Chem. Soc. Rev.* **2018**, *47*, 5125−5145.

(3) Che, F.; Gray, J. T.; Ha, S.; Kruse, N.; Scott, S. L.; McEwen, J.-S. Elucidating the Roles of Electric Fields in Catalysis: A Perspective. *ACS Catal.* **2018**, *8*, 5153−5174.

(4) Ciampi, S.; Darwish, N.; Aitken, H. M.; Díez-Pérez, I.; Coote, M. L. Harnessing electrostatic catalysis in single molecule, electro-

chemical and chemical systems: a rapidly growing experimental tool box. *Chem. Soc. Rev.* **2018**, *47*, 5146−5164.

(5) Shaik, S.; Danovich, D.; Joy, J.; Wang, Z.; Stuyver, T. Electric-Field Mediated Chemistry: Uncovering and Exploiting the Potential of (Oriented) Electric Fields to Exert Chemical Catalysis and Reaction Control. *J. Am. Chem. Soc.* **2020**, *142*, 12551−12562.

(6) Stuyver, T.; Danovich, D.; Joy, J.; Shaik, S. External electric field effects on chemical structure and reactivity. *Wiley Interdiscip. Rev.: Comput. Mol. Sci.* **2020**, *10*, No. e1438.

(7) Aragonès, A. C.; Haworth, N. L.; Darwish, N.; Ciampi, S.; Bloomfield, N. J.; Wallace, G. G.; Diez-Perez, I.; Coote, M. L. Electrostatic catalysis of a Diels-Alder reaction. *Nature* **2016**, *531*, 88−91.

(8) Oshima, K.; Shinagawa, T.; Haraguchi, M.; Sekine, Y. Low temperature hydrogen production by catalytic steam reforming of methane in an electric field. *Int. J. Hydrogen Energy* **2013**, *38*, 3003−3011.

(9) Oshima, K.; Shinagawa, T.; Nogami, Y.; Manabe, R.; Ogo, S.; Sekine, Y. Low temperature catalytic reverse water gas shift reaction assisted by an electric field. *Catal. Today* **2014**, *232*, 27−32.

(10) Sekine, Y.; Tomioka, M.; Matsukata, M.; Kikuchi, E. Catalytic degradation of ethanol in an electric field. *Catal. Today* **2009**, *146*, 183−187.

(11) Gray, J. T.; Agarwal, K.; Cho, J.-H.; Yang, J.-I.; Ha, S. Estimating surface electric fields using reactive formic acid probes and SEM image brightness analysis. *Chem. Eng. J.* **2020**, *402*, 125640.

(12) Che, F.; Gray, J. T.; Ha, S.; McEwen, J.-S. Improving Ni Catalysts Using Electric Fields: A DFT and Experimental Study of the Methane Steam Reforming Reaction. *ACS Catal.* **2017**, *7*, 551−562.

(13) Che, F.; Gray, J. T.; Ha, S.; McEwen, J.-S. Reducing Reaction Temperature, Steam Requirements, and Coke Formation During Methane Steam Reforming Using Electric Fields: A Microkinetic Modeling and Experimental Study. *ACS Catal.* **2017**, *7*, 6957−6968.

(14) Shih, C. F.; Zhang, T.; Li, J.; Bai, C. Powering the Future with Liquid Sunshine. *Joule* **2018**, *2*, 1925−1949.

(15) Trimm, D. L.; Önsan, Z. I. Onboard fuel conversion for hydrogen-fuel-cell-driven vehicles. *Catal. Rev.* **2001**, *43*, 31−84.

(16) Sá, S.; Silva, H.; Brandão, L.; Sousa, J. M.; Mendes, A. Catalysts for methanol steam reforming-A review. *Appl. Catal. B* **2010**, *99*, 43−57.

(17) Cai, F.; Ibrahim, J. J.; Fu, Y.; Kong, W.; Zhang, J.; Sun, Y. Low-temperature hydrogen production from methanol steam reforming on Zn-modified Pt/MoC catalysts. *Appl. Catal. B* **2020**, *264*, 118500.

(18) Agrell, J.; Birgersson, H.; Boutonnet, M. Steam reforming of methanol over a Cu/ZnO/Al2O3 catalyst: a kinetic analysis and strategies for suppression of CO formation. *J. Power Sources* **2002**, *106*, 249−257.

(19) Cheng, Z.; Jiang, C.; Sun, X.; Lan, G.; Wang, X.; He, L.; Li, Y.; Tang, H.; Li, Y. Insights into the Inducing Effect of Aluminum on Cu-ZnO Synergy for Methanol Steam Reforming. *Ind. Eng. Chem. Res.* **2022**, *61*, 11699−11707.

(20) Wang, Z.; Danovich, D.; Ramanan, R.; Shaik, S. Oriented-External Electric Fields Create Absolute Enantioselectivity in Diels-Alder Reactions: Importance of the Molecular Dipole Moment. *J. Am. Chem. Soc.* **2018**, *140*, 13350−13359.

(21) Olah, G. A. Beyond Oil and Gas: The Methanol Economy. *Angew. Chem., Int. Ed.* **2005**, *44*, 2636−2639.

(22) Ke, C.; He, W.; Liu, S.; Ru, X.; Liu, S.; Lin, Z. Multiscale Catalyst Design for Steam Methane Reforming Assisted by Deep Learning. *J. Phys. Chem. C* **2021**, *125*, 10860−10867.

(23) Han, Z.-K.; Sarker, D.; Ouyang, R.; Mazheika, A.; Gao, Y.; Levchenko, S. V. Single-atom alloy catalysts designed by first-principles calculations and artificial intelligence. *Nat. Commun.* **2021**, *12*, 1833.

(24) Fu, Z.; Yang, B.; Wu, R. Understanding the Activity of Single-Atom Catalysis from Frontier Orbitals. *Phys. Rev. Lett.* **2020**, *125*, 156001.

(25) Chen, L. D.; Urushihara, M.; Chan, K.; Nørskov, J. K. Electric Field Effects in Electrochemical CO2 Reduction. *ACS Catal.* **2016**, *6*, 7133−7139.

(26) Michaelides, A.; Liu, Z.-P.; Zhang, C. J.; Alavi, A.; King, D. A.; Hu, P. Identification of General Linear Relationships between Activation Energies and Enthalpy Changes for Dissociation Reactions at Surfaces. *J. Am. Chem. Soc.* **2003**, *125*, 3704−3705.

(27) Abild-Pedersen, F.; Greeley, J.; Studt, F.; Rossmeisl, J.; Munter, T. R.; Moses, P. G.; Skúlason, E.; Bligaard, T.; Nørskov, J. K. Scaling Properties of Adsorption Energies for Hydrogen-Containing Molecules on Transition-Metal Surfaces. *Phys. Rev. Lett.* **2007**, *99*, 016105.

(28) Kresse, G.; Furthmüller, F. Efficient iterative schemes forab initiototal-energy calculations using a plane-wave basis set. *Phys. Rev. B* **1996**, *54*, 11169−11186.

(29) Kresse, G.; Furthmüller, F. Efficiency of ab-initio total energy calculations for metals and semiconductors using a plane-wave basis set. *Comput. Mater. Sci.* **1996**, *6*, 15−50.

(30) Blöchl, P. E. Projector augmented-wave method. *Phys. Rev. B* **1994**, *50*, 17953−17979.

(31) Perdew, J. P.; Wang, Y. Accurate and simple analytic representation of the electron-gas correlation energy. *Phys. Rev. B* **1992**, *45*, 13244−13249.

(32) Neugebauer, J.; Scheffler, M. Adsorbate-substrate and adsorbate-adsorbate interactions of Na and K adlayers on Al(111). *Phys. Rev. B* **1992**, *46*, 16067−16080.

(33) Henkelman, G.; Uberuaga, B. P.; Jónsson, H. A Climbing Image Nudged Elastic Band Method for Finding Saddle Points and Minimum Energy Paths. *J. Chem. Phys.* **2000**, *113*, 9901−9904.

(34) Henkelman, G.; Jónsson, H. A dimer method for finding saddle points on high dimensional potential surfaces using only first derivatives. *J. Chem. Phys.* **1999**, *111*, 7010−7022.

(35) Ke, C.kechangming/DL-accelerated-catalysis-design: v1.0.0. 2022; https://doi.org/10.5281/zenodo.7008915, (accessed on Oct 12, 2022).

(36) Yeh, C.-H.; Pham, T. M. L.; Nachimuthu, S.; Jiang, J.-C. Effect of External Electric Field on Methane Conversion on IrO2(110) Surface: A Density Functional Theory Study. *ACS Catal.* **2019**, *9*, 8230−8242.

(37) Pacchioni, G.; Lomas, J. R.; Illas, F. Electric field effects in heterogeneous catalysis. *J. Mol. Catal. A: Chem.* **1997**, *119*, 263−273.

(38) Che, F.; Ha, S.; McEwen, J.-S. Elucidating the field influence on the energetics of the methane steam reforming reaction: A density functional theory study. *Appl. Catal. B* **2016**, *195*, 77−89.

(39) Campbell, C. T.; Mao, Z. Analysis and prediction of reaction kinetics using the degree of rate control. *J. Catal.* **2021**, *404*, 647−660.

(40) Valdés-Solís, T.; Marbán, G.; Fuertes, A. Nanosized catalysts for the production of hydrogen by methanol steam reforming. *Catal. Today* **2006**, *116*, 354−360.

(41) Twigg, M. V.; Spencer, M. S. Deactivation of Copper Metal Catalysts for Methanol Decomposition, Methanol Steam Reforming and Methanol Synthesis. *Top. Catal.* **2003**, *22*, 191.

(42) Liu, Z.; Yao, S.; Johnston-Peck, A.; Xu, W.; Rodriguez, J. A.; Senanayake, S. D. Methanol steam reforming over Ni-CeO2 model and powder catalysts: Pathways to high stability and selectivity for H2/CO2 production. *Catal. Today* **2018**, *311*, 74−80.